1 Laser Applications for Future High-Energy and High-Intensity Accelerators

Ralph Assmann (CERN), Weiren Chou (Fermilab), Eric Esarey (LBNL),
Dino Jaroszynski (U. of Strathclyde), Yun Liu (ORNL), Tor Raubenheimer (SLAC),
Mike Seidel (PSI), Toshiki Tajima (LMU MPQ) and Kaoru Yokoya (KEK)

1.1 Introduction

The consensus in the world high-energy physics community is that the next large collider after the LHC will be a TeV-scale lepton collider. Options currently under study include the ILC (0.5-1 TeV), CLIC (up to 3 TeV) and the muon collider (up to 4 TeV), all using RF technology. On the other hand, the very high gradients (~10 GeV/m) possible with laser acceleration open up new avenues to reach even higher energy and more compact machines. At this workshop participants discussed and set forth a set of beam and laser parameters for a 1-10 TeV e^+e^- collider based on two different technologies – laser plasma acceleration (LPA) and direct laser acceleration (DLA). Because the effectiveness of a collider is judged by its luminosity, and the cross section for a process creating a large mass M varies as $1/M^2$, a high energy machine must also have high luminosity. The luminosity goal for a 10 TeV collider is 10^{36} $cm^{-2}s^{-1}$, a factor of 100 higher than for a 1 TeV machine. To reach this goal, the laser system must have high average power (~100 MW) and high repetition rate (kHz to MHz).

Moreover, the laser-based collider must have high wall-plug efficiency in order to keep power consumption at a reasonable level. To set this efficiency goal, the workshop compared the efficiency of a number of large accelerators, either in operation or in a design phase. The results are listed in Table 1. Our goal is 10% for an LPA

Table 1: Comparison of wall-plug efficiency of various accelerators.

Accelerator	Beam	Beam energy (GeV)	Beam power (MW)	Efficiency AC to beam	Note on AC power
PSI Cyclotron	H+	0.59	1.3	0.18	RF + magnets
SNS Linac	H^-	0.92	1.0	0.07	RF + cryo + cooling
TESLA (23.4 MV/m)	e^+/e^-	250 × 2	23	0.24	RF + cryo + cooling
ILC (31.5 MV/m)	e^+/e^-	250 × 2	21	0.16	RF + cryo + cooling
CLIC	e^+/e^-	1500 × 2	29.4	0.09	RF + cooling
LPA	e^+/e^-	500 × 2	8.4	0.10	Laser + plasma

It is difficult to set a reasonable goal for cost. Ideally, the cost of a collider based on laser technology should be significantly lower than colliders based on conventional RF technology in order to make this new technology attractive. Take the 0.5 TeV ILC as an example. The total estimated cost is about $8B, of which about 1/3 is the RF cost. This gives roughly $5M per GeV for RF. The laser cost of a LPA or DLA collider should be an order of magnitude lower in order to be competitive.

The workshop also studied the laser requirements for a 200 GeV γγ collider. This idea originated at BINP is based on the consideration that the cross section for Higgs production in a γγ collider is significantly larger than an e^+e^- collider of the same energy. In 2008, it was proposed to the ICFA to build a 180 GeV γγ collider as the first stage of a full scale ILC in order to lower the construction cost and realize a more rapid start for the project. This proposal was not approved for a number of reasons: physics potential, cost saving potential, need for additional laser R&D. This workshop concluded that, as a matter of fact, the required laser systems for an ILC γγ collider may already be within reach of today's technology, whereas for a CLIC γγ collider the required laser technology could piggyback on the inertial fusion project LIFE at LLNL or the high power laser project ELI in Europe (see Sec. 1.4).

In addition to high-energy colliders, lasers also find application at another frontier – high-intensity accelerators. Lasers have been used in beam diagnostics for some time now, including beam profile monitor ("laser wire") and beam polarization measurement. These require only low power lasers. A challenge, however, is to use a laser for stripping H^- particles during injection into a high-intensity proton machine, such as the SNS, J-PARC or Project X. In these MW-scale machines, the thin foils made of carbon or diamond that have been used for stripping would experience a severe heating problem and have limited lifetime. Experiments have demonstrated that a laser beam interacting with H^- particles can convert them to protons. However, to replace foils in real machine operation, the laser must have high average power (kW) and high repetition rate (hundreds of MHz). This workshop investigated the required laser parameters for the SNS and Project X.

1.2 1-10 TeV e^+e^- Colliders Based on Laser Plasma Acceleration

Advanced acceleration techniques are actively being pursued to expand the energy frontier of future colliders. Although the minimum energy of interest for the next lepton collider will be determined by high-energy physics experiments presently underway, it is anticipated that ≥1 TeV center-of-mass energy will be required. Laser-plasma accelerators are one promising technique for reducing the size and cost of future colliders, provided the needed laser technology is developed.

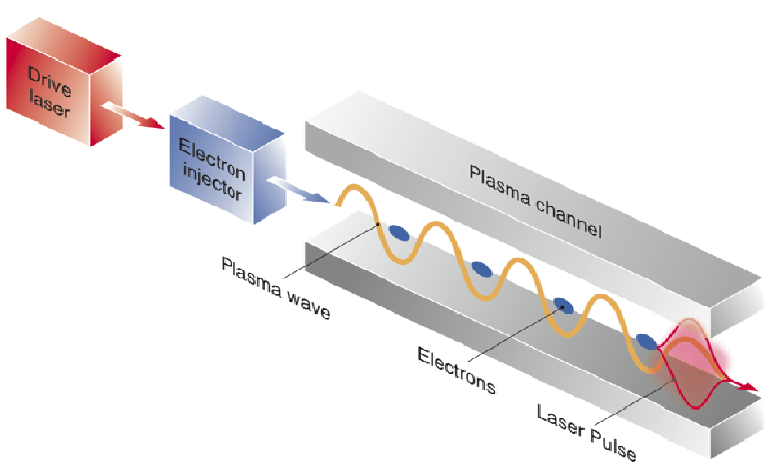

Figure 1: Laser-plasma acceleration: An intense laser pulse drives a plasma wave (wake) in a plasma channel, which also guides the laser pulse and prevents diffraction. Plasma background electrons that are injected with the proper phase can be accelerated and focused by the wake [1].

Laser-plasma accelerators (LPAs) are of great interest because of their ability to sustain extremely large acceleration gradients, thus resulting in compact accelerating structures [1-3]. Laser-plasma acceleration is realized by using a short-pulse, high-intensity laser to ponderomotively drive a large electron plasma wave (or wakefield) in an underdense plasma (see Fig. 1). The electron plasma wave has relativistic phase velocity, approximately the group velocity of the laser, and can support large electric fields in the direction of propagation of the laser. When the laser pulse is approximately resonant (duration on the order of the plasma period) and the laser intensity is relativistic (with normalized laser vector potential $a_0 = eA/m_ec^2 \sim 1$), the magnitude of the accelerating field is on the order of $E_0[\mathrm{V/m}] = 96(n_0[\mathrm{cm}^{-3}])^{1/2}$, and the wavelength of the accelerating field is on the order of the plasma wavelength $\lambda_p[\mu\mathrm{m}] = 3.3\times10^{10}(n_0[\mathrm{cm}^{-3}])^{-1/2}$, where n_0 is the ambient electron number density. For example, $E_0 \approx 30$ GeV/m (approximately three orders of magnitude beyond conventional RF technology) and $\lambda_p \approx 100$ μm for $n_0 = 10^{17}$ cm^{-3}. Rapid progress in laser-plasma accelerator research, and in particular the demonstration of high-quality GeV electron beams over cm-scale plasmas at Lawrence Berkeley National Laboratory [4] has increased interest in laser-plasma acceleration as a path toward a compact TeV-class linear collider [5]. A conceptual diagram of a LPA-based collider is shown in Fig. 2.

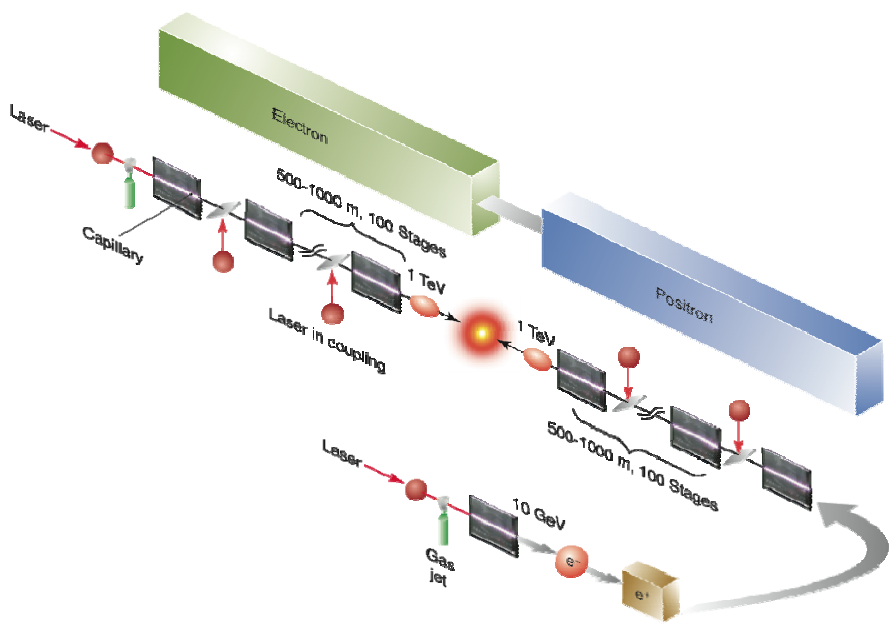

Figure 2: Concept for a LPA-based electron-positron collider. Both the electron and positron arms start with a plasma-based injection-acceleration module where controlled injection techniques are applied to produce a high quality ~10 GeV electron beam. Electrons are then accelerated to 1 TeV using 100 laser-plasma modules, each consisting of a 1-m long preformed plasma channel (10^{17} cm^{-3}) driven by a 30 J laser pulse giving a 10 GeV energy gain. A fresh laser pulse is injected into each module. Similarly, positrons are produced from a 10 GeV electron beam through pair creation and then trapped and accelerated in a LPA module to ~10 GeV. Subsequent LPA modules would accelerate positrons to 1 TeV. A luminosity of 10^{34} cm^{-2}s^{-1} requires 4×10^9 particles/bunch at a 13 kHz repetition rate [1].

In the standard laser wakefield acceleration configuration, the electron plasma wave is driven by a nearly resonant laser (pulse duration on the order of the plasma period) propagating in a neutral, underdense ($\lambda_p >> \lambda$, where λ is the laser wavelength) plasma. There are several regimes of plasma acceleration that can be accessed with a laser driver. Two regimes that have attracted attention for collider applications are the quasi-linear regime [3] and the bubble [6] (or blow-out [7]) regime. The quasi-linear regime is accessible for parameters such that $\pi^2 r_L^2 / \lambda_p^2 >> a_0^2/2\gamma_L$, where a_0^2 can be written as a function of the laser intensity I_0; $a_0^2 = 7.3\times10^{-19}(\lambda\ [\mu m])^2\ I_0[W/cm^2]$ (linear polarization), $\gamma_L = (1+a_0^2/2)^{1/2}$, and r_L is the laser spot size. The amplitude of the accelerating field of the plasma wave in the quasi-linear regime is $E_z \approx 0.76(a_0^2/2\gamma_L)E_0$. This regime is characterized by regular plasma wave buckets and nearly-symmetric regions of acceleration-deacceleration and focusing-defocusing (see Fig. 3). In the quasi-linear regime, the accelerating and focusing phase regions for electrons and positrons are symmetric since the wakefield is approximately sinusoidal.

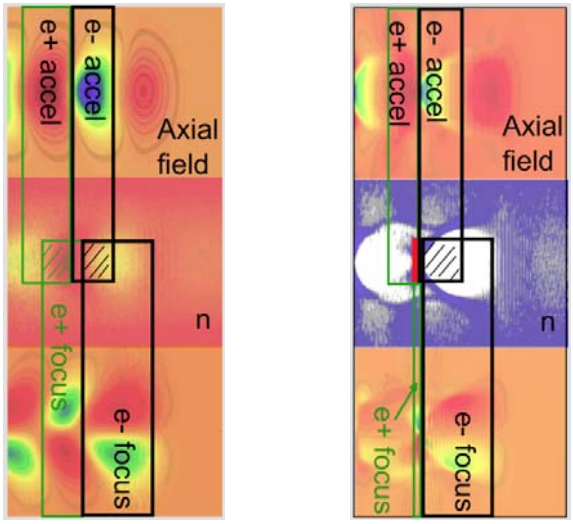

Figure 3: Wakes generated in the quasi-linear (left) and bubble (right) regimes by a laser pulse with a_0=1 (left) and a_0=4 (right). Top figures are axial electric field, central figures are density, and bottom figures are transverse electric fields. The black boxes indicate the accelerating/focusing regions for electrons, and the green boxes are for positrons (courtesy C.G.R. Geddes *et al.*, LBNL).

The bubble regime of LPA occurs for laser-plasma parameters such that $\pi^2 r_L^2 / \lambda_p^2 << a_0^2/2\gamma_L$. This regime is characterized by complete removal of plasma electrons and creation of an ion cavity (see Fig. 3). The bubble regime has several attractive features for acceleration of electron beams. Inside the moving ion cavity, the focusing forces for electrons are linear (and attractive) and uniform for all phases and the accelerating field is independent of transverse position with respect to the cavity axis. The major drawback of accessing the highly-nonlinear bubble regime is that acceleration of positrons is problematic because the entire ion cavity is defocusing for positrons, and a positron beam will be scattered transversely. There does exist a small phase region immediately behind the bubble where positrons could be accelerated and

focused; however, here some of the attractive properties of the bubble regime (e.g., uniform accelerating and constant linear focusing) are lost.

The amount of charge that can be accelerated in a plasma wave is determined by the plasma density and the size of the accelerating field. The maximum charge that can be loaded is given by the number of charged particles required to cancel the laser excited wake (beam loading limit). A collider will operate with asymmetric shaped particle bunches such that bunches can be loaded with charge near the beam loading limit without a large wake-induced energy spread. The maximum number of loaded charged particles into a small ($<< \lambda_p = 2\pi/k_p$) segment is approximately $N = n_0 k_p^{-3} (E_z/E_0)$.

In general, the energy gain in a single laser-plasma accelerator stage may be limited by laser diffraction effects, dephasing of the electrons with respect to the accelerating field phase velocity (approximately the laser driver group velocity), and laser energy depletion into the plasma wave. Laser diffraction effects can be mitigated by use of a plasma channel (transverse plasma density tailoring), guiding the laser over many Rayleigh ranges. Dephasing can be mitigated by plasma density tapering (longitudinal plasma density tailoring), which can maintain the position of the electron beam at a given phase of the plasma wave. Ultimately, the single-stage energy gain is determined by laser energy depletion. The energy depletion length scales as $L_d \sim \lambda_p^3/\lambda^2 \propto n_0^{-3/2}$ and the energy gain in a single stage scales with plasma density as $W_{stage} \approx E_z L_d \propto n_0^{-1}$.

After a single laser-plasma accelerating stage, the laser energy is depleted and a new laser pulse must be coupled into the plasma for further acceleration. This coupling distance is critical to determining the overall accelerator length (set by the average, or geometric, gradient of the main linac) and the optimal plasma density at which to operate. One major advantage of laser-driven plasma acceleration is the potential for a short coupling distance between stages, and, therefore, the possibility of a high average (geometric) accelerating gradient and a relatively short main linac length. Although conventional laser optics might require meters of space to focus intense lasers into subsequent LPA stages, plasma mirrors show great promise as optics to direct high-intensity laser pulses, requiring only tens of cm to couple a drive laser into a plasma accelerator stage. A plasma mirror uses overdense plasma creation by the intense laser on a renewable surface (e.g., metallic tape or liquid jet) to reflect the laser beam. Reducing the main linac length requires the coupling length between stages to be on the order of the length of a single plasma acceleration stage.

The beam-beam interaction at the interaction point (IP) of a collider produces radiation (beamstrahlung) that generates background for the detectors and increases the beam energy spread (resulting in loss of measurement precision). The beam-beam interaction is characterized by the Lorentz-invariant beamstrahlung parameter Υ (mean field strength in the beam rest frame normalized to the Schwinger critical field). The current generation of linear collider designs based on conventional technology operate in the classical beamstrahlung regime $\Upsilon << 1$. Next generation linear colliders (≥1 TeV) will most likely operate in the quantum beamstrahlung regime with $\Upsilon >> 1$. In the quantum beamstrahlung regime, the average number of emitted photons per electron scales as $n_\gamma \propto \Upsilon^{2/3}$ and the relative energy spread induced scales as $\Delta E_\gamma \propto \Upsilon^{2/3}$. Assuming that the center of mass energy, luminosity, beam power, and beam sizes are fixed, $n_\gamma \propto (N\sigma_z)^{1/3}$ and $\Delta E_\gamma \propto (N\sigma_z)^{1/3}$, where σ_z is the particle bunch length [5]. In this regime, beamstrahlung is reduced by using shorter

bunches and smaller charge per bunch. Laser-plasma accelerators are intrinsically sources of short (fs) electron bunches, due to shortness of the plasma wavelength λ_p.

Tables 2A and 2B show estimates of parameters for electron-positron colliders for three cases: a 1 TeV CoM collider with a plasma density of $n_0 = 10^{17}$ cm^{-3}, a 10 TeV CoM collider with a plasma density of $n_0 = 10^{17}$ cm^{-3} (Scenario I in Table 2), and a 10 TeV CoM collider with a plasma density of $n_0 = 10^{18}$ cm^{-3} (Scenario II in Table 2). In all these cases a laser wavelength of $\lambda = 1$ μm and an intensity 3×10^{18} W/cm^2 ($a_0 = 1.5$) is assumed. The laser-plasma accelerator parameters are based on scaling laws for the quasi-linear regime obtained from simulation codes. A mild plasma density taper is assumed. The length of one linac is on the order of 0.1 km for the 1 TeV, $n_0 = 10^{17}$ cm^{-3} case and of the order 1 km for the 10 TeV, $n_0 = 10^{17}$ cm^{-3} case. The conversion efficiencies assumed are 50% for laser to plasma wave and 40% for plasma wave to beam (laser to beam is 20%). A high laser wall plug efficiency of 50% is also assumed, giving an overall wall plug to beam efficiency of 10%. Notice that the laser energy per stage per bunch is on the order of tens of J (for $n_0 = 10^{17}$ cm^{-3}) and the required rep-rates are of the order of tens of kHz (for $n_0=10^{17}$ cm^{-3}), clearly indicating the need for the development of laser systems with high average power (hundreds of kW) and high peak power (hundreds of TW). The higher rep-rate (170 kHz) and higher total wall power (3.4 GW) required for the higher plasma density case ($n_0 = 10^{18}$ cm^{-3}) is less favourable than the $n_0 = 10^{17}$ cm^{-3} case.

A process that extracts the energy of the remaining wakefields in the plasma has been suggested [8]. Inserting circuitry in the plasma as a passive feedback system extracts the wakefield energy, converts this energy into electric energy, and feeds it into an external circuit. The conversion efficiency is on the order of unity. Thus, it would enhance the coupling efficiency of the laser pulse to the wakefield energy by at least a factor of 2 (or even more).

Table 2A: Beam parameters of 1 TeV and 10 TeV e^+e^- colliders based on LPA technology.

Case	**1 TeV**	**10 TeV (Scenario I)**	**10 TeV (Scenario II)**
Energy per beam (TeV)	0.5	5	5
Luminosity (10^{34} cm^{-2}s^{-1})	1.2	71.4	71.4
Electrons per bunch ($\times10^9$)	4	4	1.3
Bunch repetition rate (kHz)	13	17	170
Horizontal emittance $\gamma\varepsilon_x$ (nm-rad)	700	200	200
Vertical emittance $\gamma\varepsilon_y$ (nm-rad)	700	200	200
β* (mm)	0.2	0.2	0.2
Horizontal beam size at IP σ^*_x (nm)	12	2	2
Vertical beam size at IP σ^*_y (nm)	12	2	2
Luminosity enhancement factor	1.04	1.35	1.2
Bunch length σ_z (μm)	1	1	1
Beamstrahlung parameter Υ	148	8980	2800
Beamstrahlung photons per electron n_γ	1.68	3.67	2.4
Beamstrahlung energy loss δ_E (%)	30.4	48	32
Accelerating gradient (GV/m)	10	10	10
Average beam power (MW)	4.2	54	170
Wall plug to beam efficiency (%)	10	10	10
One linac length (km)	0.1	1.0	0.3

Table 2B: Laser and plasma parameters of 1-10 TeV e^+e^- colliders based on LPA technology.

Case	**1 TeV**	**10 TeV (Scenario I)**	**10 TeV (Scenario II)**
Wavelength (μm)	1	1	1
Pulse energy/stage (J)	32	32	1
Pulse length (fs)	56	56	18
Repetition rate (kHz)	13	17	170
Peak power (TW)	240	240	24
Average laser power/stage (MW)	0.42	0.54	0.17
Energy gain/stage (GeV)	10	10	1
Stage length [LPA + in-coupling] (m)	2	2	0.06
Number of stages (one linac)	50	500	5000
Total laser power (MW)	42	540	1700
Total wall power (MW)	84	1080	3400
Laser to beam efficiency (%) [laser to wake 50% + wake to beam 40%]	20	20	20
Wall plug to laser efficiency (%)	50	50	50
Laser spot rms radius (μm)	69	69	22
Laser intensity (W/cm^2)	3×10^{18}	3×10^{18}	3×10^{18}
Laser strength parameter a_0	1.5	1.5	1.5
Plasma density (cm^{-3}), with tapering	10^{17}	10^{17}	10^{18}
Plasma wavelength (μm)	105	105	33

1.3 10 TeV e^+e^- Colliders Based on Direct Laser Acceleration

The Direct Laser Acceleration (DLA) research effort focuses on development of high-gradient dielectric-loaded vacuum accelerator structures driven with high-repetition rate tabletop near-infrared lasers. The concept is to use dielectric structures to couple very-high laser fields to a particle beam much in the way that microwave structures are used to couple RF fields to a beam except that the wavelength and dimensions are reduced by a factor of 10,000 (from cm to μm). The dielectric structure confines a speed-of-light optical mode that is driven by a laser and will accelerate synchronous charged particles as shown in Figure 4. In contrast to plasma-coupling schemes, structure-based acceleration offers strong coupling to the particle beam, and is fundamentally a linear acceleration process. Consequently, laser pulse energies in the <1 μJ/pulse range are needed to generate GeV/m-class gradients, the process has no minimum laser energy threshold, and efficient energy transfer between laser and particle beam is possible [9]. Lasers with the required peak and average power, and >30% wall-plug efficiency are commercially available. The technology to integrate much of the accelerator infrastructure onto a single silicon or silica substrate (an "accelerator chip") exists today and is being advanced rapidly by industry. The program leverages the private sector's multi-billion dollar investments in semiconductor and telecommunication technology to produce an entirely new accelerator technology.

The primary challenges for this technology are the requirement of exquisite phase control of multiple lasers and the reduction in the dimensions from microwave-scales to near-IR that lead to very small machine apertures. Since carrier-phase

envelope methods were proposed in 1999, significant progress in optical phase stabilization of ultrashort lasers has occurred, leading to microwave-reference frequency combs for optical metrology, and to the efficient, coherent combination of the outputs of multiple lasers [10]. The small apertures require constructing the accelerator structures with micron-scale dimensions. Three styles of structures are being considered: photon band-gap fibers [11], a 3-D band-gap 'woodpile' structure [12], and a grating structure [13]. The small dimensions also require small bunch charge and small emittances which is also naturally required by optimum beam loading and beam transport considerations. As optimum beam loading bunch charges are on the order of 10 fC, the pulse repetition rate must be dramatically raised to provide sufficient beam power to attain adequate luminosity. Fortunately, repetition rates in the tens of megahertz range are natural for fiber lasers and allow for bunch-by-bunch feedback systems that will be necessary to maintain beam control.

Beam transport though the small aperture requires very small normalized emittances. In a manner similar to RF accelerators, microscale periodic focusing elements will play an important role for beam containment in the structure vacuum channel. Simple beam transport considerations have led us to a possible FODO lattice for beam transport in a PBG fiber accelerator. Focusing elements of 2 cm length, 1 mm bore, and a gradient of ~500 T/m spaced ~2 m apart would allow for transport of a beam with an emittance of $\sim 10^{-10}$ m-rad through a ~1.5 λ aperture typical for these near-field structures. While 0.1 pm is a very small normalized emittance, it corresponds to a phase space density of $N/\varepsilon = 4\times10^{14}$ e/m, well below the 6×10^{15} e/m densities routinely achieved today from photo-injector sources [14].

Early laser acceleration experiments were performed on the Stanford University campus (Figure 5), and in 2007 the same collaboration moved to SLAC with the development of the E163 test facility in the NLCTA. Recent successes include demonstration of attosecond bunch train formation [15] and the first demonstration of the staging of two laser accelerator sections driven at optical wavelengths [16]. The future program will explore the technical limits to laser acceleration, including gradient, acceptance and emittance preservation, and apply semiconductor and fiber-optic manufacturing techniques to demonstrate an entirely new class of structures. Tables 3A and 3B list parameters for a 10 TeV CoM DLA collider. It is important to note that the intrinsically small bunch charge leads to cleaner beam collisions than any other approach considered thus far and may make the DLA technique the only reasonable choice at such very high energy-scales.

Table 3A: Beam parameters of a 10 TeV e^+e^- collider based on DLA technology.

Energy per beam (TeV)	5
Luminosity (10^{34} cm^{-2}s^{-1})	105
Electrons per bunch ($\times 10^9$)	0.002
Bunch repetition rate (kHz)	25000
Horizontal emittance $\gamma\varepsilon_x$ (nm-rad)	0.1
Vertical emittance $\gamma\varepsilon_y$ (nm-rad)	0.1
Horizontal beam size at IP σ^*_x (nm)	0.064
Vertical beam size at IP σ^*_y (nm)	0.064
Bunch length σ_z (μm)	335
Beamstrahlung parameter Υ	0.377
Beamstrahlung photons per electron n_γ	0.52
Beamstrahlung energy loss δ_E (%)	4.37
Accelerating gradient (GV/m)	0.5
Average beam power (MW)	39
Wall plug to beam efficiency (%)	10
One linac length (km)	10

Table 3B: Laser parameters of a 10 TeV e^+e^- collider based on DLA technology.

Wavelength (μm)	8.0
Pulse energy/stage (nJ)	240
Pulse length (μm)	1740
Repetition rate (kHz)	25,000
Peak power (kW)	17
Average laser power/stage (kW)	10
Energy gain/stage (GeV)	1.3
Stage length [LPA + in-coupling] (m)	2.6
Number of stages (one linac)	3900
Total laser power (MW)	156
Total wall power (MW)	390
Wall plug to laser efficiency (%)	40
Laser spot rms radius (μm)	16
Laser intensity (W/cm^2)	6.4×10^9
Laser strength parameter a_0	1.2×10^{-3}

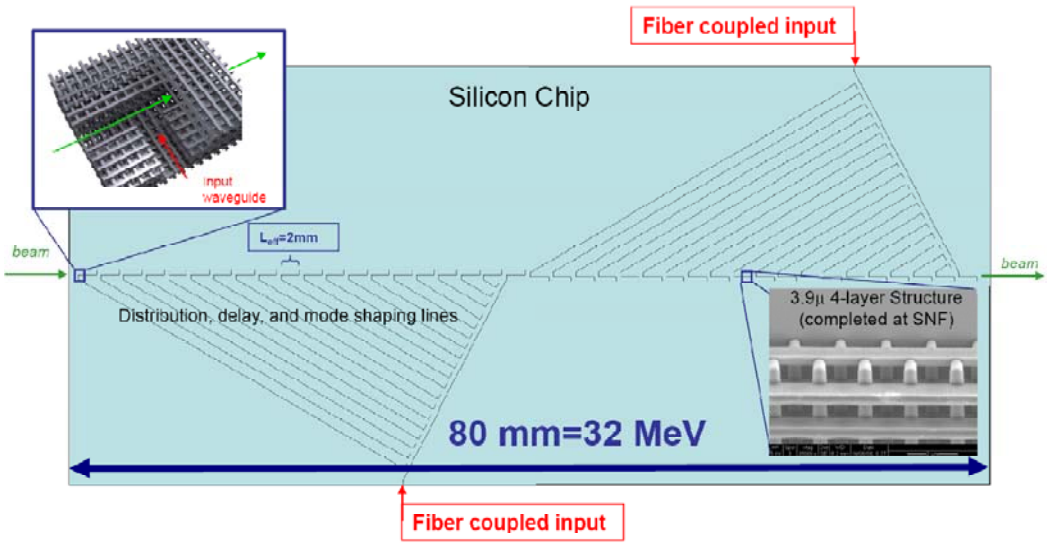

Figure 4: Cartoon showing an integrated silicon woodpile accelerator structure composed of 40 woodpile accelerating structures powered from two fiber lasers. At known damage fluences for 2 mm light, 32 MeV energy gain in 8 cm is expected. Cutaway of coupler region (inset, upper left, courtesy B. Cowan, Tech-X), and SEM image of fabricated silicon woodpile lattice (inset, lower right, courtesy C. McGuinness, Stanford).

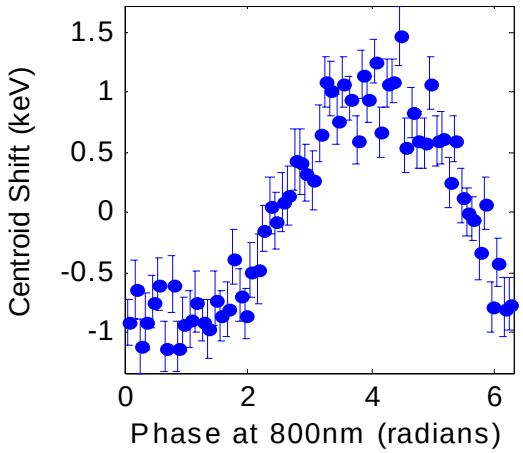

Figure 5: Experimental observation of optical acceleration of optically bunched electrons. The sinusoidal variation of energy of all ~350 optical bunches with the phase of the accelerator is plainly visible. Bunches are prepared by the IFEL process, and accelerated by the inverse transition radiation process. Maximum observed gradient 6 MeV/m is due to low coupling efficiency of ITR process; near-field structures are expected to yield a factor of ~100 better gradient.

1.4 200 GeV γγ Colliders

An electron-electron linear collider can be converted to a photon-photon collider by converting the electron beams into photon beams by irradiating laser beams just before the collision point as shown in Figure 6.

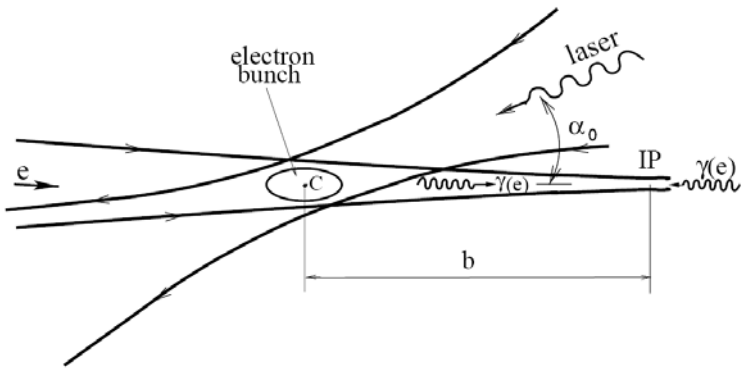

Figure 6: Illustration of the principle of a γγ collider.

This scheme opens the possibility for investigating different physics from the collider than when it is operating with charged particle beams. The wave length λ_L of the laser should be as short as possible for creating high energy photons from a given electron energy. However, it must satisfy

$$\lambda_L\,[\mu m] > \sim 4\ E_e[TeV]$$

where E_e is the electron energy, because, otherwise, the created high-energy photons would be lost by electron-positron pair creation in the same laser beam. To obtain a narrow photon energy spectrum the laser beam should be circularly polarized (and electrons longitudinally polarized). Linear polarization may sometimes be needed depending on the physics processes being studied.

Since the transverse electron beam size at the conversion point is much smaller than the laser spot size, the probability of conversion is almost entirely determined by the laser parameters and is independent of the electron parameters as long as the electrons go through the entire length of the laser pulse. For almost all the electrons to be converted into photons, the required flash energy of the laser pulse is approximately given by

$$A = \omega_L * \sigma_C/S_L$$

where ω_L is the laser photon energy, σ_C the cross section of Compton scattering, and S_L the effective cross section of the laser beam. S_L cannot be too small due to the Rayleigh length requirement. Thus, in any case A is about a few Joules. On the other hand, the required pulse structure of the laser beam, which must match the electron beam, strongly depends on the collider design. In particular, a superconducting collider (e.g. ILC) and a normal-conducting collider (e.g., CLIC) demand very different pulse structures. The pulse structure can be characterized by a few parameters: n_b the number of bunches in a train, t_b the interval between bunches, n_b*t_b the train length, and f_{rep} the repetition frequency of the trains. The train length is O(ms) for superconducting colliders but is O(μs) or less for a normal-conducting collider.

Table 4 shows examples of the required laser parameters for low-energy (Low-mass Higgs region) γγ colliders based on the ILC and CLIC parameters. The parameters for the ILC is based on those given by V. Telnov [17] slightly modified

according to the present ILC parameters [18]. The parameters for CLIC are based on the proposal CLICHÉ [19] with the updated parameters of CLIC [20]. V. Telnov made important correction to some of the CLIC parameters as well as provided the laser parameters. [21] (For the ILC a possible use of FEL is proposed [22] but this is irrelevant in the present context.)

All of these parameters are subject to change depending on the project evolution as well as on the optimization of the interaction region. Owing to the long bunch train (980 μs) and large bunch spacing (370 ns) for the ILC it is possible to use an optical cavity for accumulating the laser power (the multiplication factor Q in the table) so that the requirements for the laser are greatly relaxed at the cost of very high precision optical system [23]. This type of optical cavities is similar to that currently under construction for a Compton x-ray source at KEK [24].

For the CLIC it would be difficult to employ an optical cavity because the bunch train is short (177 ns) and the bunch spacing small (0.5 ns). However, the required laser system is similar to a single laser beam line of the Laser Inertial Fusion Energy (LIFE) project at LLNL in the US. This laser beam line has an output energy of >10 kJ per pulse at a repetition rate >10 Hz, or an average laser power >100 kW. (LIFE project would need a total of 192 lines.) The amplifier is capable to deliver a pulse of 177 ns. A modified front end can readily split a continuous pulse to 354 short pulses of 5 J each. Given appropriate funding, LLNL could put together a 10 kJ module that is diode pumped within 3 years [25]. The main difference between LIFE and CLIC is the repetition rate (10 Hz *vs.* 50 Hz). This problem could be solved by replacing Nd:glass by ceramic Nd:YAG, which would allow the repetition rate to be increased to >50 Hz. Technology similar to this has also been proposed for the Extreme Light Infrastructure (ELI) project in Europe [26].

Table 4: Beam and laser parameters of γγ colliders.

Electron Beam Parameters	**ILC**	**CLIC**
Energy per electron beam (GeV)	100	100
Max energy of photons (GeV)	60 (75)	60
γγ luminosity at the high energy peak (10^{34} cm^{-2}s^{-1})	0.13	0.19
Electrons per bunch (× 10^{10})	2	0.68
Number of bunches in a train (n_b)	2640	354
Distance between bunches (t_b, ns)	370	0.5
Length of the train (n_b*t_b , μs)	980	0.177
Repetition frequency ($f_{rep,}$ Hz)	5	50
Electron bunch length σ_z (μm)	300	44
Normalized emittance $\varepsilon_{x/y}$ (mm-mrad)	10/0.035	1.4/0.050
Beta-function at IP $\beta_{x/y}$ (mm)	4/0.3	2/0.02
Beam size $\sigma_{x/y}$ (nm)	450/7.3	120/2.3
Distance between conversion point and IP (mm)	~1.5	~0.5
Crossing angle (mrad)	25	25
Laser Parameters		
Wavelength (μm)	1 (0.5)	1
Rayleigh range (mm), f#	~0.5, 20	~0.4,18
Laser pulse energy (J)	~10/Q	5
Pulse length (r.m.s., ps)	~1.5	~1
Peak power (TW)	~2.5/Q	2
Average power (kW)	150/Q	90
Laser power in a train (MW)	25/Q	10000
Cavity enhancement factor	Q~300	1

Notes on Table 4: (by V. Telnov)

1) Distance between the Compton conversion point (CP) and the interaction point (IP) is $b = \gamma\sigma_y$.
2) Thickness of the laser target is equal to 1.2 collision lengths.
3) Luminosity in the high energy peak means $L_{\gamma\gamma}(W > 0.8W_{max})$
4) For the ILC, the numbers are given for $\lambda = 1$ μm. Those in ( ) are for $\lambda = 0.5$ μm.
5) For the ILC, $\lambda = 1$ μm is OK and $\lambda = 0.5$ μm may be possible. But for CLIC only $\lambda = 1$ μm is allowed because the disruption angle is 1.5 times larger. [The disruption angle is proportional to $(N/\sigma_z)^{1/2}$.]
6) "Undulator" parameter $\xi^2 = 0.15$ (0.2) was used for $\lambda = 1$ (0.5) μm, corresponding to reduction of W_{max} by 5%.

1.5 Laser Stripping of H^- Particles in High-Intensity Proton Accelerators

1.5.1 Laser Stripping of H^- Particles for SNS

The Spallation Neutron Source (SNS) utilizes charge-exchange injection to "stack" a high-intensity proton beam in the accumulator ring for short-pulse neutron production. In this process, a 1 ms long H^- beam pulse is transported to a carbon stripping foil located at the injection point of the ring. The electrons are stripped and the resulting proton is merged with previously accumulated beam. This injection scheme is central to the operation of many facilities, including the SNS, J-PARC, ISIS and PSR.

As the beam power of the SNS is increased from the 1.44 MW design to more than 3 MW as envisioned in the SNS Power Upgrade project, the stripping foils become radioactive and produce uncontrolled beam loss, which is one of the main factors limiting beam power in high intensity proton rings.

A "foil-less" charge exchange injection method was first proposed in the 1980s by using a field dissociation process. This scheme requires an impractically large laser power, which is indeed the central difficulty involved in ionizing neutral hydrogen. Recently, ORNL scientists came up with a three-step scheme for laser stripping.

An H^- ion has two electrons. The first electron is loosely bound with a binding energy of 0.7 eV, whereas the second one is tightly bound with a binding energy of 13.6 eV. The ORNL 3-step scheme works as follows: First, H^- ions are converted to H^0 by stripping off the first electron in a magnetic field; then H^0 atoms are excited from the ground state ($n = 1$) to the upper levels ($n \geq 3$) by a laser, and the excited states H^{0*} are converted to H^+ by stripping the second electron in a second magnetic field.

In a proof-of-principle experiment, a third harmonic beam from a Q-switched laser was used for stripping. The laser generates a 30 Hz, 6 ns pulses with a peak power of ~10 MW at 355 nm. The stripping efficiency reached 90%. The positive result has encouraged us to proceed in developing a real scheme for SNS stripping. Such a system will need to reach an efficiency of 98%, similar to that of conventional foils.

A simple multiplication of 10 MW laser peak power, used in the first experiments, and the duty factor of the SNS beam (6%) yields an average laser power of 0.6 MW at 355 nm to strip the entire ion beam. Obviously, this power is too large to make the device practical. Therefore, a number of approaches have been investigated to mitigate the requirement of peak/average laser power.

1) Optimization of H^- beam parameters

   An appropriate dispersion derivative of the H^- beam will be designed to eliminate the Doppler broadening of the absorption line width and therefore to reduce the required frequency sweep for the laser beam. The vertical size as well as the horizontal angular spread of the H^- beam will be minimized. The optimization of the H^- beam parameters will reduce required peak power of the laser to the 1 MW level. Reduction of the bunch length of the ion beam can further reduce the average laser power requirement.

2) Macropulse laser system

   At SNS, the H^- beam consists of approximately 50-ps long micropulses separated by ~2.5 ns and gated into mini-pulses 650 ns long. The period of minipulses, or a turn, is determined by the SNS accumulation ring beam path length (~1 μs) and the beam energy. The minipulses are bunched into macropulses with a length of 1 ms and a repetition rate of 60 Hz. In order to achieve high efficiency laser stripping, the laser pulses need to overlap with each ion beam micropulse at the interaction point. The ideal (minimum laser power requirement) condition would be that the laser pulses have an identical temporal structure as the H^- beam. A prototype of such a macropulse laser system has been developed in collaboration with Continuum Inc. It includes a mode-locked seed laser, a pulse picker, multi-stage solid-state amplifiers, and harmonic generation crystals to convert infrared beam to UV light. The challenge of the macropulse laser system is the high repetition rate and over 1 ms macropulse duration.

3) Beam recycling optical resonator

   The photon-hydrogen interaction results in a negligible loss to the laser beam power; it is expected that the average power of the laser can be significantly reduced by recycling the laser beam with an optical resonator. Different cavity configurations including Fabry-Perot, ring cavity, or cavity with built-in harmonic generation crystals need to be investigated. Optical resonator technology is well developed for low-power, infrared, and often continuous laser beams. However, for the SNS the resonator needs to work on a high intensity UV laser beam. In addition, since the photon-hydrogen interaction has to occur inside the resonator, the optics need to operate within a high vacuum and its control electronics need to survive in an environment with high radiation dose. These constraints pose severe technical challenges in the development of the optical resonator.

Table 5A lists the parameters of the SNS H^- beam and Table 5B summarizes the required laser parameters with and without the beam recycling optical resonator.

Table 5A: SNS H^- beam parameters.

Beam energy (GeV)	1.0 (upgrade: 1.3)
Beam power (MW)	1.4 (upgrade: 3.0)
Beam macropulse length (ms)	1.0
Beam micropulse length (ps)	50
Peak macropulse H- current (mA)	38
Ring accumulation time (turn)	1060
Ring bunch intensity	1.6×10^{14}
Vertical size (mm)	0.6
Vertical emittance (mm-mrad)	0.225π
Horizontal size (mm)	3
Vertical emittance (mm-mrad)	0.225π

Table 5B: Required laser parameters for SNS laser stripping.

Method	**Macropulse laser**	**Macropulse laser w/ 20x resonator**
Laser wavelength (nm)	355	355
Micropulse length (ps)	50	50
Micropulse energy (μJ)	50	2.5
Micropulse repetition rate (MHz)	402.5	402.5
Macropulse length (ms)	1	1
Macropulse energy (J)	20	1
Macropulse repetition rate (Hz)	60	60
Average power (W)	1200	60
Temporal profile	Flat	Flat
Contrast	N/A	N/A
Efficiency	Normal solid-state lasers	Normal solid-state lasers
Polarization	100/1	100/1
Cost	Multi $M	Multi $M
Laser beam quality	$M^2 < 1.2$	$M^2 < 1.2$
Pulse stability	1%	1%
Laser pointing stability (μrad)	1	1
Laser availability	24/7	24/7

1.5.2 Laser Stripping of H^- Particles for Project X

Project X would convert H^- particles to protons at 8 GeV. This has the advantage of using a laser of longer wavelength because the photon energy would be increased by the relativistic γ factor (γ = 9.526) due to the Doppler shift. The beam parameters are listed in Table 6 and the beam pulse structure is shown in Figure 7.

Table 6: Project X H^- beam parameters.

Kinetic energy (GeV)	8
Relativistic γ	9.526
Micropulse length (ps)	15 ps
Micropulse frequency (MHz)	325
Micropulse period (ns)	3.1
Macropulse length (ms)	1.25
Macropulse current (mA)	20
Macropulse frequency (Hz)	5
No. H^- per micropulse	4×10^8
No. micropulses per macropulse	4×10^5
No. H^- per macropulse	1.6×10^{14}
No. H^- per second	8×10^{14}
Vertical beam size (mm)	1.5
Horizontal beam size (mm)	1.5
Beam power (MW)	1

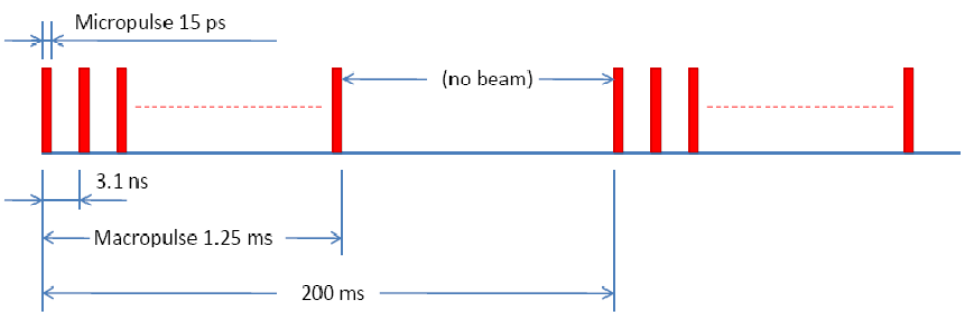

Figure 7: H^- pulse structure of Project X.

1.5.2.1 *Direct Laser Ionization*

The photoionization of the ground state of the hydrogen atom H(1s) has been studied extensively in the past half century. For low intensity radiation there are exact expressions of this process in terms of the cross section obtained from the perturbation theory [27]. In this approximation, the incident photon flux density is much smaller than 1 atomic unit (a.u.) and the pulse duration is much longer than an optical cycle. However, this approximation is no longer valid when intense laser pulses are employed, since the peak electric fields can be comparable with or larger than 1 a.u. and the pulse may last only a few optical cycles or even a fraction of a cycle. Therefore, perturbative methods are not applicable and numerical methods for solving the time-dependent Schrödinger equation (TDSE) are required.

Ionization of hydrogen atoms by intense laser pulses is a complex subject that is still not fully understood [28-30]. Although many theoretical approaches have been proposed, they typically break down at high laser intensities or neglect important aspects of the laser-atom interaction such as long-range Coulomb interaction or realistic pulse shapes. On the other hand, numerical solutions of the TDSE provide accurate predictions, but are extremely computationally intensive and converge

slowly at high intensities. Current results show that no simple relationship links ionization rate to pulse duration, frequency and intensity, due to competing ionization mechanisms, evolving energy levels, resonances and stabilization.

Calculations performed for 24.8 nm (50 eV), 2.5 fs (30 periods) pulses suggest that intensities beyond 10^{17} W/cm^2 are required for efficient (> 90%) ionization of hydrogen atoms [31]. From an experimental standpoint, few absolute measurements of the ionization yield are available. An experiment performed with 600 fs, 248 nm laser pulses measured ~0.001% ionization for intensities of the order of 10^{14} W/cm^2 [32].

1.5.2.2 *Three-Step Stripping*

Electrons in hydrogen atoms exposed to intense laser radiation can be excited to higher states. For the Project X parameters, the n = 2 transition can be triggered when the hydrogen beam interacts with a 1024 nm laser beam at an angle of ~96 degree. A laser peak power of ~3.5 MW is required for 90% stripping.

It may be possible to reduce the required laser energy by decreasing the incidence angle (Figure 8). However, this approach can only be investigated by performing detailed simulations of the response of hydrogen atoms to the laser field.

Counter-propagating geometry would require a laser at around 1.8 μm, which could be achieved using an OPA. However, detailed calculations would be required to establish the powers required and the role of Stark Shifting, etc.

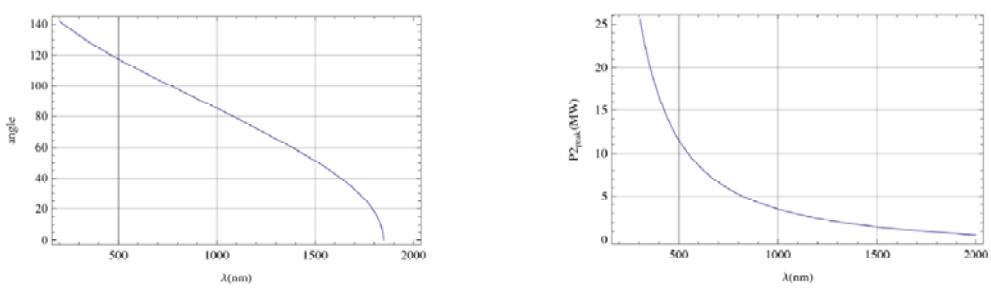

Figure 8: Wavelength *vs.* angle and power *vs.* wavelength required for ionization of hydrogen atoms.

1.6 Acknowledgements

Carl Schroeder and Wim Leemans (LBNL) contributed to the writing of Section 1.2. Valery Telnov (BINP), Chris Barty (LLNL) and Wolfgang Sandner (MBI) made important comments in Section 1.4. Enrico Brunetti (U. of Strathclyde) contributed to Section 1.5.2.

1.7 References

1. W.P. Leemans and E. Esarey, *Physics Today* **62**, 44 (2009).
2. T. Tajima and J.M. Dawson, *Phys. Rev. Lett.* **43**, 267 (1979).
3. E. Esarey, C.B., Schroeder, W.P. Leemans, *Rev. Modern Phys.* **81**, 1229 (2009).
4. W.P. Leemans *et al*., *Nature Physics* **2**, 696 (2006).
5. C.B. Schroeder *et al*., in Proc 2008 Advanced Accelerator Concepts Workshop, edited by C. B. Schroeder, E. Esarey, and W. Leemans, AIP Conf. Proc. **1086** (Amer. Inst. Phys., NY, 2009), p. 208.

6. A. Pukhov and J. Meyer-ter-Vehn, *Appl. Phys.* **B 74**, 355 (2002).
7. W. Lu et al., *Phys. Rev. ST Accel. Beams* **10**, 061301 (2007).
8. T. Tajima and A. Chao, private communication.
9. R. H. Siemann, "Energy efficiency of laser driven, structure based accelerators", *Phys. Rev. ST Accel. Beams* **7**, 061303, (2004); see also N. Na, *et al.*, "Energy efficiency of an intracavity coupled, laser-driven linear accelerator pumped by an external laser", *Phys. Rev. ST Accel. Beams* **8**, 031301, (2005).
10. W. Liang, A. Yariv, A. Kewitsch, G. Rakuljic, "Coherent combination of semiconductor lasers using optical phase-lock loops", *Opt. Lett.*, **32** (4), p.370, (2007).
11. X. E. Lin, "Photonic band gap accelerator", *Phys. Rev. ST Accel. Beams* **4**, 051301, (2001).
12. B. Cowan, "Three-dimensional dielectric photonic crystal structure for laser-driven acceleration", *Phys. Rev. ST Accel. Beams* **11**, 011301, (2008); see also C. McGuinness, *et al.*, "Accelerating electrons with lasers and photonic crystals", *J. Modern Optics*, **56** (18&19), p.2142ff, (2009).
13. T. Plettner, *et al.*, "Proposed few optical cycle laser driven particle accelerator structure", *Phys. Rev. ST Accel. Beams* **9**, 111301, (2006); see also T. Plettner, R.L. Byer, "Proposed dielectric-based microstructure laser-driven undulator," *Phys. Rev. ST Accel. Beams* **11**, 030704 (2008).
14. E. Colby *et al.*, "An electron source for a laser accelerator", *in Proc. 2003 Part. Accel. Conf.*, p.2101-2103, (2003).
15. C. M. S. Sears *et al.*, "Production and characterization of attosecond bunch trains", *Phys. Rev. ST Accel. Beams*, **11**, 061301, (2008).
16. C. M. S. Sears *et al.*, "Phase stable net acceleration of electrons from a two-stage optical accelerator", *Phys. Rev. ST Accel. Beams*, **11**, 101301, (2008).
17. Private communication.
18. RDR, http://www.linearcollider.org/about/Publications/Reference-Design-Report
19. D. Asner *et.al.*, "Higgs physics with a γγ collider based on CLIC 1", *Eur. Phys. J. C* **28**, 27–44 (2003)
20. R. Tomas, "Overview of the Compact Linear Collider", *Phys. Rev. ST Accel. Beams* **13**, 014801 (2010). Two parameter sets for E_{CM} = 0.5 and 3 TeV are given. Here, the former is used.
21. Private communication.
22. For example, E. Saldin *et al.*, Proc. PAC2009, Vancouver, BC, Canada, WE6PFP083.
23. For example, G. Klemz *et al.*, "Design study of an optical cavity for a future photon collider at ILC", *Nucl. Instr. Meth.* **A564**, 212 (2006).
24. J. Urakawa, "Development of a compact x-ray source based on Compton scattering using 1.3 GHz superconducting RF accelerating linac and a new laser storage cavity", submitted to *Nucl. Instr. Meth.* **A**.
25. C. Barty, private communication.
26. W. Sandner, private communication.
27. H. A. Bethe and E. E. Salpeter, *Quantum Mechanics of One- and Two-Electron Atoms*, pp 295-322, Springer-Verlag (1957).
28. A. N. Grum-Grzhimailo *et al.*, *Phys. Rev.* **A 81**, 043408 (2010).
29. S. Borbély *et al.*, *Phys. Rev.* **A 77**, 033412 (2008).
30. S. Geltman, *J. Phys. B: At. Mol. Opt. Phys.* **33**, 1967 (2000).
31. J. Bauer *et al.*, *J. Phys. B: At. Mol. Opt. Phys.* **34**, 2245 (2001).
32. G. A. Kyrala and T. D. Nichols, *Phys. Rev.* **A 44**, R1450–R1453 (1991).